The evolution of a coastal carbon store over the last millennium

Craig Smeaton[1*], Xingqian Cui[2], Thomas S. Bianchi[3], Alix G. Cage[4], John A. Howe[5], William E.N. Austin[1,5].

[1] School of Geography & Sustainable Development, University of St Andrews, St Andrews, KY16 9AL, UK

[2] School of Oceanography, Shanghai Jiao Tong University, 1954 Huashan Road, Xuhui Siat, Shanghai, China.

[3] Department of Geological Sciences, University of Florida, Gainesville, FL 32611, USA

[4] School of Geography, Geology and the Environment, Keele University Staffordshire, ST5 5BG, UK

[5] Scottish Association for Marine Science, Oban, PA37 1QA, UK

Corresponding author: Craig Smeaton (cs244@st-andrews.ac.uk)

Highlights

- Fjord sediments are highly responsive OC sinks adapting to changing pressures.
- Human disturbance in the catchment drives aged terrestrial OC input to the fjord.
- OCAR over the last 500 years have risen by 20% driven by anthropogenic disturbance.
- Climate preconditions catchments increasing their sensitivity to human disturbance

Keywords: carbon; fjords; sediment; anthropogenic; human; climate; mid-latitude; coastal; radiocarbon

Abstract

Fjord sediments are recognized as hotspots for the burial and storage of organic carbon, yet little is known about the long-term drivers of significant terrestrial organic carbon (OC) transfers into these coastal carbon stores. The mid-latitude fjord catchments of Scotland have a long history of human occupation and environmental disturbance. We provide new evidence to show that increased anthropogenic disturbances over the last 500 years appear to have driven a step change in the magnitude of terrestrial OC transported to the coastal ocean. Increased pressures from mining, agriculture and forestry over the latter half of the last millennium have destabilized catchment soils and remobilized deep stores of aged OC from the catchment to the coastal ocean. Here we show that fjord sediments are capable of acting as highly responsive and effective terrestrial OC sinks, with OC accumulation rates increasing up to 20 % during the peak period of anthropogenic disturbance. The responsiveness and magnitude of the fjord OC sink represents a potentially significant time-evolving component of the global carbon cycle that is currently not recognized but has the potential to become increasingly important in the understanding of the role of these coastal carbon stores in our climate system.

1. Introduction

Fjords are locations of high sediment deposition and despite representing a relatively small area of the global continental margin (<0.1%), they contain ~ 12% of the sediments deposited over the past 100,000 years (Syvitski et al., 1987). The glacially-deepened basins of fjords (Bianchi et al., 2020; Howe et al., 2002), in tandem with their location and the land-ocean interface, allow significant quantities of organic carbon (OC) to be trapped and stored over centennial to millennial periods (Bianchi et al., 2018; Skei, 1983). Globally, fjords are estimated to bury 18 Mt OC yr^{-1}, which is equivalent to ca. 11% of the annual marine carbon burial (Hedges and Keil, 1995; Smith et al., 2015). Moreover, 55 to 62% of the OC buried in fjords originates from terrestrial sources (Cui et al., 2016b).

The mid-latitude fjords of Scotland are no different to their global counterparts, with postglacial sediments estimated to hold 252.4 ± 62 Mt of OC (Smeaton et al., 2017). The majority of OC stored is found in the muddy sediments (Smeaton et al., 2021; Smeaton and Austin, 2019), with between 52 to 65% of the OC in surficial sediments originating from terrestrial sources (Smeaton and Austin, 2017). Unlike the vegetated fjords of New Zealand, Chile, and Alaska, the catchments of the mid-latitude fjords of NW Europe have a long history of human occupation and evidence of environmental disturbance (Smout, 2004; Tipping, 2013; Winchester, 1996), potentially driving increased OC export from the terrestrial environment to the fjord sediments.

The role of fjords as nationally and globally important carbon (C) sinks is now well established (Smith et al., 2015), yet the drivers and evolution of OC burial and storage in these coastal systems remains largely unknown. Here, we present a sediment record from Loch Sunart, a fjord on the west coast of Scotland (Fig.1) and attempt to explain the role that anthropogenic disturbance played over the last millennium in the development of the sedimentary C store, and for the wider significance of long-term C burial in such fjord environments. The geomorphological and oceanographic features that allow fjords to trap and store significant quantities of OC are also ideal for reconstructing regional climate conditions (Cage and Austin, 2010; Faust et al., 2016; Sepúlveda et al., 2009), and potentially human activity within the catchment (Zillén et al., 2008; Zillén and Conley, 2010).

2. Study Site

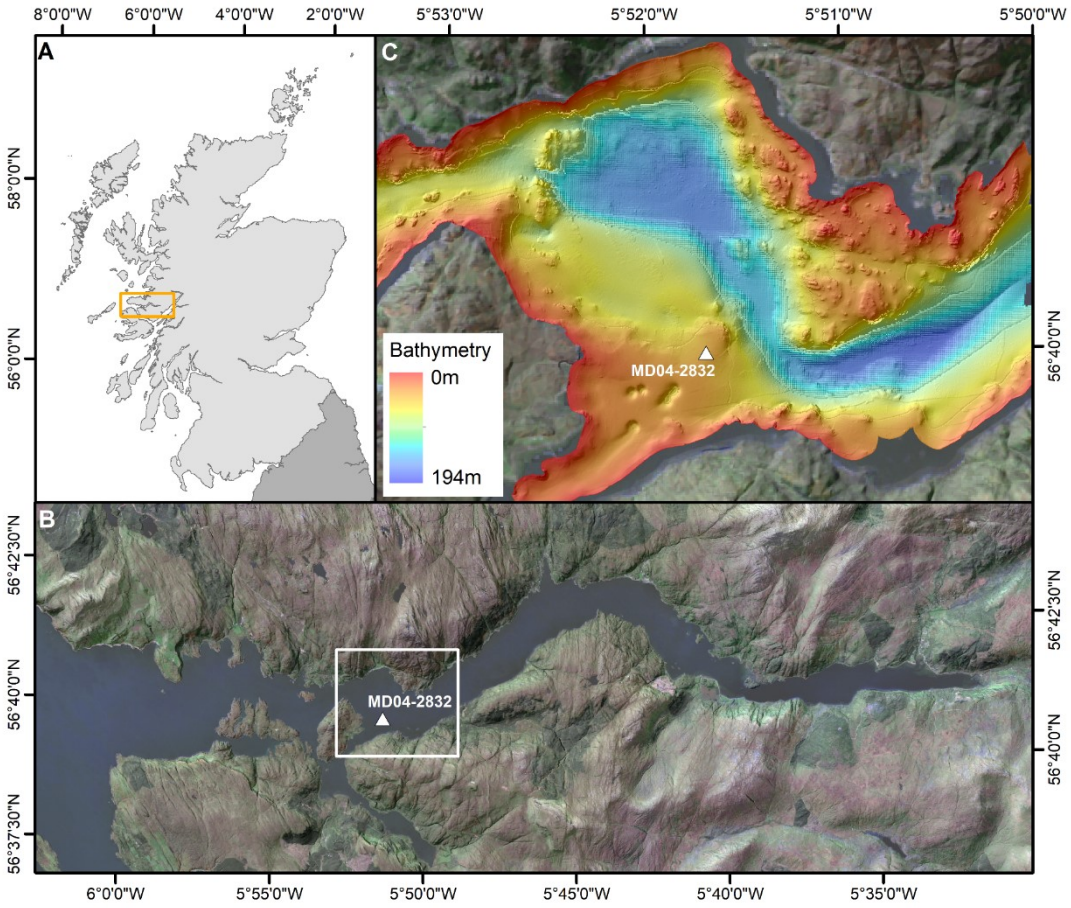

Figure 1. Location of **(A)** Loch Sunart on the NW coast of Scotland **(B)** Coring site in the context of Loch Sunart **(C)** Sampling site of core MD04-2832 displayed with the seabed bathymetry (accessed from the United Kingdom Hydrographic Office https://datahub.admiralty.co.uk). Landscape imagine (Sentinel 2, 2019) accessed from www.digimap.edina.ac.uk.

Loch Sunart is a temperate non-glaciated fjord on the west coast of Scotland (Fig.1). The fjord is 30.7 km long and has an areal extent of 47.3 km^2 with a maximum depth of 145 m and consists an outer, middle, and upper basin separated by shallow rock sills at depths of 31 m and 6 m, respectively. Loch Sunart's catchment covers 299 km^2 and is dominated by shallow (mean depth: 50 cm) C-rich, peaty gley soil and a land cover largely consisting of acid grasslands, commercial coniferous and deciduous woodlands (Smeaton and Austin, 2017). The physical characteristics of Loch Sunart and its catchment are largely representative of fjords across mainland Scotland (Smeaton et al., 2017); the fjords of mainland Scotland have comparable

physical characteristics to the vegetated fjords found on the Norwegian mainland, Canada, and New Zealand (Bianchi et al., 2020; Howe et al., 2010; Syvitski et al., 1987).

The oceanographic conditions of Loch Sunart, and most other Scottish fjords, are well ventilated bottom waters that generally experience only minor seasonally hypoxic events (Gillibrand et al., 2005). Recent calculations estimate the post-glacial sediments of Loch Sunart store 9.4 ± 0.2 Mt of OC (Smeaton et al., 2016), with an estimated 42.0 ± 10.1 % of the OC held within the surface sediments derived from terrestrial sources (Smeaton and Austin, 2017).

Loch Sunart's catchment and the surrounding areas have a long record of human occupation. (Smout, 2004; Tipping, 2013; Winchester, 1996), extending back to the early Viking presence (~850 AD), and progressive regional environmental disturbances arising from intensification the of grazing (1350 AD), wide-spread woodland removal (1400-1600 AD), the introduction of lead mining (1722 AD) and start of industrial forestry (1927 AD). Key events in the catchment's history are summarized in Figure 2.

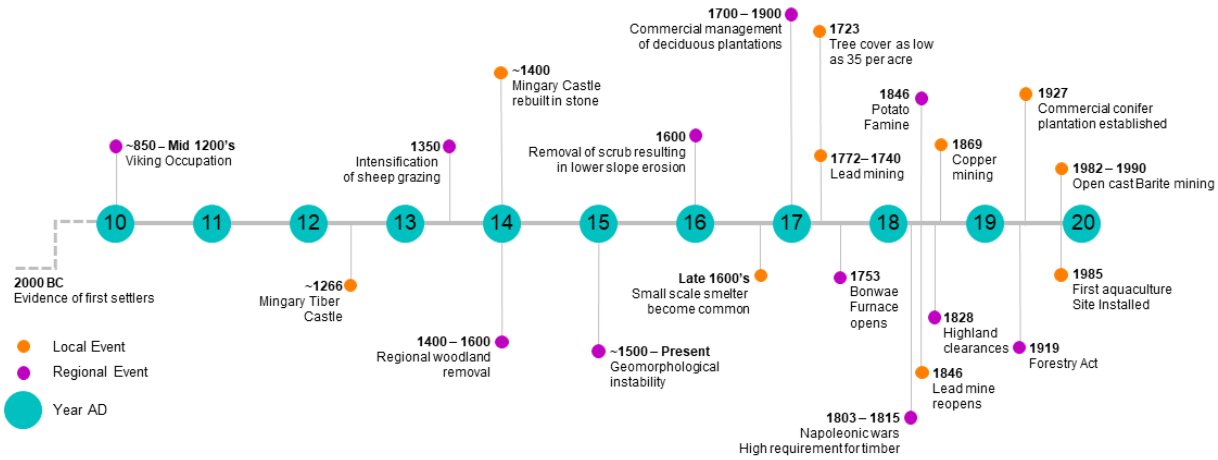

Figure 2. Timeline of key events pertaining to human occupation and disturbance in the Sunart region (Ballantyne, 1991; Bishop et al., 2015; Brazier and Ballantyne, 1989; Smout, 2005, 2004, 2003; Tipping, 2013, 1994; Winchester, 1996).

3. Materials and Methods

3.1 Sampling

A 22.5 m giant piston core MD04-2832 (56.669833, -5.868667) was collected from the research vessel *Marion Dufresne* in the middle basin of Loch Sunart in 2004 (Fig.1) from a

water depth of 52.1 m. In addition to core MD04-2832, a 6m gravity core PM06-GC01 (56.670000, -5.871833) and a multi-core PM06-MC01 (56.670000, -5.871667) were collected from the research vessel *Prince Madog* at same site in 2006 (Cage and Austin, 2010).

3.2 Physical Properties Analysis

Core MD04-2832 was split on-board the *RV Marion Dufresne*, photographed and described using the Folk classification scheme (Folk, 1954) (see supplementary material). Upon return to the University of St Andrews, volumetric samples (5 cm^3) were taken at 5 cm intervals from the core using a modified syringe sampler. The mass of the wet sample was recorded prior to freeze drying. Once dried, samples were reweighed - allowing for water content (%), wet and dry bulk density (g cm^{-3}), and porosity (Φ) of sediments to be determined (see methods in Dadey et al., 1992; Danielson and Sutherland, 1986). Magnetic susceptibility was measured using a multi-sensor core logger on-board the RV *Marion Dufresne.*

3.3 Geochemical Analysis

3.3.1 Radiocarbon Analysis

Fourteen *in-situ* paired bivalve shells (*Corbula varicorbula and Nucula sulcata)* and one benthic foraminifera (multi-species) sample were collected from cores MD04-2832, PM06-GC01 and PM06-MC01C (Table 1) for radiocarbon dating (Cage and Austin, 2010). A further 10 bulk sediment samples underwent radiocarbon analysis to estimate the age of the OC (Table 2).

Prior to analysis, mollusc shells, and foraminifera were washed with DI water to remove any organic residue then were etched (20% by weight removal of outer layer) with 1M hydrochloric acid (HCl). Milled samples were placed in a pre-cleaned Pyrex® hydrolysis unit (Ascough et al., 2005). Carbon dioxide (CO_2) was evolved from the shells and the foraminifera by hydrolysis with 85% phosphoric acid (H_3PO_4) under vacuum. The bulk sediment samples were moistened with a small amount of deionised water, covered by glass fibre filters and placed into a glass vessel together with a beaker of concentrated HCl to hydrolyse any $CaCO_3$ in the sample over 3 days (Bao et al., 2019; Harris et al., 2001). The total carbon in a known weight of the pre-treated sample was recovered as CO_2 by combustion on a Costech, Elemental Analyser.

The evolved CO_2 from the shells, foraminifera and bulk sediments was converted to graphite by the Fe/Zn reduction (Xu et al., 2007). Sample graphites were analysed using AMS at Aarhus

University (AAR) and the NERC Radiocarbon Facility (SUERC). Radiocarbon results are expressed as conventional radiocarbon ages (year BP) and fraction modern (F_{modern}) based on the equation: $F_{modern} = (\Delta^{14}C/1000 + 1)/(e^{(-\lambda * (\text{collection year}—1950))})$, where λ and $\Delta^{14}C$ are the decay constant and radiocarbon compositions, while collection year is reported as the calendar year.

The ages of shell and benthic foraminifera samples were calibrated using OxCal 4.4 (Ramsey and Lee, 2013) with the Marine20 curve (Heaton et al., 2020) and a regional correction of ΔR value of −26 ± 14 yr (Cage et al., 2006). Bulk sediment ages are reported as conventional ^{14}C ages. To determine the age of OC at the point of deposition, the deposition age (derived from the shell based age model) was subtracted from the bulk sediment age.

3.3.1.1 Core Chronology

An age model for the core site MD04-2832 was developed using the 14 calibrated ^{14}C the mollusc shell ages from Cores MD04-2832, PM06-GC01 and PM06-MC01. Magnetic susceptibility measurements were used to assure the different cores were comparable: full details of the core correlation process is outlined in Cage and Austin (2010). Additionally, a ^{210}Pb chronology (Appleby, 2002) developed for core PM06-MC01 (Suppl. Table 1; Cage and Austin, 2010) was utilised in the creation of the age model. An age model was created using the calibrated ^{14}C dates and the ^{210}Pb data in the BACON software package (Blaauw and Christen, 2011). To test the age model comparisons were made to an additional ^{14}C age acquired from benthic foraminiferal from a core depth of 305 cm and the Landnám tephra layer (871 ± 2 Cal BP) located at a depth of 320-325 cm in adjacent core MD04-2831 (Cage et al., 2011).

3.3.2 Elemental and Stable Isotope Analysis

Elemental (OC, N) and stable isotope analyses ($\delta^{13}C_{org}$ and $\delta^{15}N$) of the sediments were carried out. The freeze-dried samples were milled to a fine powder, with ~12 mg placed into both tin and sliver capsules. The tin capsules were analysed to determine N concentration while the silver capsules underwent acid fumigation (Harris et al., 2001) to remove carbonate ($CaCO_3$). Acid fumigation involves placing the silver capsules in a desiccator with a beaker of 12 M HCl for 8 hrs to remove carbonate and prevent the loss of water soluble C. Prior to analysis these samples were dried at 60°C for 24 hours. Measurements were made using an elemental analyser interfaced with an isotope ratio mass spectrometer (IRMS). C_{org} and N isotope ratios were calculated in δ notation relative to the Vienna Pee Dee Belemnite (VPDB) and Air standards respectively. Analytical precision was calculated through the repeat analysis of USGS 40

196 standard (*n = 6*) these analyses deviated from the reference values by: C = 0.08 %, N = 0.03 %,
197 $\delta^{13}C_{org}$ = 0.11 ‰ and $\delta^{15}N$ = 0.03 ‰. The C/N and N/C ratios are reported as molar ratios: C/N
198 = (OC/12)/(N/14); N/C = (N/14)(OC/12).

199 Element concentrations (As, Ba, Be, Cd, Co, Cr, Cs, Cu, Li, Mn, Mo, Ni, Pb, Rb, Sr, Th, U, V,
200 Zn) were determined using a modified version of the USEPA method 3052 (1996) for
201 microwave-assisted acid digestion of siliceous and organically based matrices. 10 ± 0.1 mg of
202 milled sediment was placed in an acid-cleaned (10% nitric acid (HNO_3)) Teflon vessel. To the
203 sediment, 2 ml of concentrated hydrogen peroxide (H_2O_2), 6 mL of concentrated HNO_3 and 2
204 mL of concentrated hydrofluoric acid (HF) were added to the sediment. The vessels were sealed
205 and transferred to the microwave digestion system (Multiwave 3000) where they remained at >
206 180 °C for more than 10 min. After digestion, samples were evaporated in a closed evaporation
207 system in a sand bath at 125 °C. Samples were cooled and transferred with 5% HNO_3 into 50
208 mL volumetric flasks. Samples were stored in polypropylene sample bottles at 4 °C until
209 analysis.

210 The elemental concentrations of the sample digests were measured by Inductively Coupled
211 Plasma–Mass Spectrometer (ICP–MS) according to USEPA method 6020A (2007). A dilution
212 factor of × 2000 was chosen for sediment samples. Each sample was measured three times. An
213 internal standard containing Indium and Bismuth (10 μg L^{-1}) was added to each sample and a
214 reference standard (Certipur® certified multi-elemental standard IV in a 6% HNO_3 matrix) was
215 run for every five samples analysed, the analytical error was estimated to be < 4 % for all
216 elements analysed. Elemental concentrations were expressed in mg kg^{-1} dry weight. Elemental
217 concentrations were normalized against the immobile element Aluminium to account for
218 dilution effects by changing sedimentary phases; this method is best suited in quantifying the
219 detrital fraction (Brumsack, 2006; Van der Weijden, 2002).

220 Quality assurance of the chemical extraction process was performed through the use of one
221 blank and a certified reference material (NCS DC75305 and NCS DC75301). Average
222 recoveries of all elements of NCS DC75305 was 92.3 ± 9.2 % (*n = 10*) and of NCS DC75301
223 was 91.7. ± 10.9 % (*n = 10*).

224 **3.3.3 Thermogravimetric analysis**

225 Thermogravimetric analysis (TGA) was carried out on all samples to quantify the lability of
226 the organic matter (OM) within the sediment. Twenty mg of milled sample was placed into 70
227 mL aluminium oxide crucible. The crucibles were placed into a Mettler Toledo TGA2 and

heated from 40 to 1000°C at a ramp heating rate of 10°C min^{-1} under a constant stream of N_2. The thermograms produced from this analysis were adjusted to a common temperature scale and clipped to the range 200-650 °C to remove interference from non-organic material. The thermograms were normalized to the mass loss, to assure all traces were comparably scaled. The first derivative of the TGA was calculated (DTG) to allow comparison of thermograms. The measured OM was grouped into three thermal fractions; labile (OM_L), recalcitrant (OM_{Recal}) and refractory (OM_{Ref}) (Capel et al., 2006). These OM fractions are thermally defined as OM_L (200 - 400 °C), OM_{Recal} (400 - 550 °C) and OM_{Ref} (550-650 °C).

3.3.4 Organic Geochemistry

Analysis of alkanes and fatty acids was based on a modified method of Cui et al. (2016a). Briefly, ~1 g samples were extracted on an accelerated solvent extractor (ASE) using dichloromethane (DCM): methanol (MeOH) (9:1 v:v). After being saponified with potassium hydroxide (KOH) in MeOH, "neutral" and "acid" fractions were sequentially extracted with hexane and hexane:DCM (4:1 v:v). The former fractions containing alkanes were analysed on the gas chromatographer – flame ionization detector (GC-FID) for alkane concentrations. The latter fraction containing fatty acids (FA) were then derivatized using boron trifloride (BF_3) in MeOH, re-extracted using DCM, and eluted using DCM on a Pasteur pipette column. Fatty acid methyl ester (FAME) samples were analysed on the same GC-FID as above.

Concentrations of alkanes and fatty acids were calculated and corrected with internal standards (C_{34} alkane isomer, C_{19} FA) and mix standards of alkanes and FAMEs. ALK $C_{25\text{-}35}$ is calculated as the sum of the odd chain C_{25} to C_{35} alkanes, while ALK $C_{24\text{-}36}$ is the sum of even chain C_{24} to C_{36} alkanes. ALK P_{aq} is the ratio of C_{23} and C_{25} alkanes over the sum of C_{23}, C_{25}, C_{29}, C_{31} alkanes. Short-chain fatty acids (SCFA) were calculated as the sum of C_{12} to C_{18} fatty acids, while long-chain fatty acids (LCFA) were calculated as the sum of C_{24} to C_{32} fatty acids. Terrestrial to aquatic ratio of fatty acids (TAR_{FA}) is the ratio of C_{24}, C_{26} and C_{28} fatty acids over the sum of C_{12}, C_{14}, C_{16}, C_{24}, C_{26}, C_{28}. Finally, the ratio of fatty acids to alkanes (FA/ALK) is the ratio of $C_{24\text{-}32}$ fatty acids to $C_{24\text{-}36}$ alkanes.

Analysis of glycerol dialkyl glycerol tetraethers (GDGTs) was based on the method of Liu et al. (2016) and Smith et al. (2010). Briefly, ~1 g of sediment samples were sonicated and extracted using DCM: MeOH (9:1 v:v) using an ultra-sonicator. The extracts were re-concentrated in hexane and analysed on a liquid chromatographer mass spectrometer (LC–MS). Quantification of GDGTs was achieved by using a synthesized tetraether surrogate standard

and focusing on targeted ions (e.g., m/z 1292) on the LC–MS. Branched/isoprenoid tetraether (BIT) index is calculated as the ratio of three branched GDGTs (I, II, and III) to the sum of branched and crenarchaeol GDGTs. The targeted m/z of the four compounds are 1022, 1036, 1050, and 1292 for branched I, II, III and crenarchaeol GDGTs.

3.4 Modelling OC contributions

To estimate the proportion of terrestrial OC (OC_{terr}) and marine (OC_{mar}) in the sediments a mixing model approach was utilised. The approach used $\delta^{13}C_{org}$, $\delta^{15}N$, N/C ratios and BIT index as tracers in conjunction with a Bayesian mixing model (Fernandes et al., 2014). The methodological approach used by Smeaton and Austin (2017) was utilised alongside the OC source characteristics specific to Loch Sunart (Suppl. Fig.6; Suppl. Table 2). The N/C ratio was chosen over the more commonly used C/N ratio, as the N/C ratio represents changes in OC rather than N (Moossen et al., 2013; Perdue and Koprivnjak, 2007). This approach does not completely overcome the problems associated with post-depositional alteration of OM, however, the use of four tracers, site specific source data, and a Bayesian approach, provided confidence in the estimates and associated errors - largely representative of the sedimentary environment. Petrogenic OC (OC_{petro}) content of the sediment was determined by comparing the total OC to the modern OC content. OC_{petro} is radiocarbon free ($F_{modern} = 0$), whereas biospheric OC, derived from terrestrial and marine sources, has variable amounts of radiocarbon ($F_{modern} > 0$). The OC_{petro} content (%) was determined by plotting the modern OC content (% OC × F_{modern}) as a function of total OC content. The point at which the linear trend of the plotted data intercepts the x-axis represents the OC_{petro} content (Cui et al., 2017; Galy et al., 2008).

3.5 Sedimentation and Carbon Accumulation

Sedimentation rates (cm yr^{-1}) were calculated using the output from the Bayesian age-depth model. The dry bulk density, porosity, and OC content were combined with the sedimentation rates over the last 1000 years to determine the mass accumulation rate (MAR) and the OC accumulation rates (OCAR), using the approach by Smith et al. (2015).

4. Results and Interpolation

4.1 Chronology

Calibrated radiocarbon dates from site MD04-2832 (Table 1) and the Bayesian age model (Suppl. Fig.3), demonstrate the upper 285 cm of MD04-2832 represents the last 1000 years. The age of the foraminiferal sample agrees well with adjacent mollusc shell dates (Table 1), indicating minimal reworking of older sediments at the site (Cage and Austin, 2010; Heier-Nielsen et al., 1995). Furthermore, the age of foraminifera and the known-age Landnám tephra layer (871 ± 2 Cal BP; Cage et al., 2011), located in adjacent core MD04-2831, are in agreement with the Bayesian age model (Suppl. Fig.3) - indicating the model is robust.

Table 1. *Calibrated radiocarbon ages of shells and foraminifera from cores MD04-2832, PM06-GC01 and PM06-MC01 produced using BACON (Blaauw and Christen, 2011) utilising radiocarbon data calibrated in OxCal 4.4 (Lienkaemper and Ramsey, 2009), using the Marine20 calibration curve (Heaton et al., 2020) with local correction of ΔR value of −26 ± 14 yr (Cage et al., 2006). Radiocarbon dates from Cage and Austin (2010). Errors reported as 1σ.*

Laboratory Code	Core	Material	Depth (cm)	^{14}C age, (yr BP)	Cal ^{14}C Age (Cal BP)
AAR-11340	PM06-MC01	*Corbula varicorbula*	28.5	476 ± 25	47 ± 38
AAR-11332	MD04-2832	*Corbula varicorbula*	35.5	485 ± 24	48 ± 39
AAR-11341	PM06-MC01	*Corbula varicorbula*	37.5	568 ± 27	33
AAR-11342	PM06-MC01	*Corbula varicorbula*	44.5	408 ± 22	40 ± 35
AAR-11343	PM06-MC01	*Corbula varicorbula*	47.5	532 ± 31	59 ± 48
AAR-11333	MD04-2832	*Corbula varicorbula*	52.5	427 ± 32	48 ± 32
AAR-11345	PM06-GC01	*Corbula sp*	62.5	550 ± 25	35
AAR-11334	MD04-2832	*Corbula varicorbula*	63.5	428 ± 26	42 ± 33
AAR-11346	PM06-GC01	*Corbula varicorbula*	92.5	674 ± 76	147 ± 90
AAR-11347	PM06-GC01	*Corbula varicorbula*	111.5	818 ± 24	281 ± 79
AAR-11336	MD04-2832	*Corbula varicorbula*	119.5	604 ± 37	39
AAR-11337	MD04-2832	*Corbula varicorbula*	137.5	686 ± 25	142 ± 75
AAR-11338	MD04-2832	*Nucula sulcata*	246.5	1167 ± 24	580 ± 51
AAR-11339	MD04-2832	*Nucula sulcata*	334.5	1687 ± 28	1081 ± 73
SUERC-12424	MD04-2832	*Mixed Benthics*	305	1511 ± 35	891 ± 5

4.2 Bulk Radiocarbon

The F_{modern} of the bulk sediment ranges between 0.74 and 0.90 at the bottom and top of the core respectively, the intermediate samples between these points have an average F_{modern} of 0.81 (Table 2). These F_{modern} values represent the quantity of ^{14}C held within the samples at present, which will be lower than that at the time of deposition. These values were corrected by subtracting the deposition age calculated from the shell derived age model (Suppl.Fig.3) from the bulk age of the sediment which in-turn allows the F_{modern} to be calculated for the sediment at the time of deposition (Table 2). It would be expected that the F_{modern} of the surface sediments would be modern in age (>1950; F_{modern} = 1), yet the 0.90 value suggests that there

316 is aged OC from the terrestrial sources in these marine sediments. The uniformity in F_{modern}
317 values below the surface of the core (11.5 -135.5 cm) indicates that the supply of aged OC_{terr}
318 to the sediments has been altered; this is likely reflective of anthropogenic induced soil erosion,
319 as opposed to a slow natural leak of aged OC.

320 ***Table 2.*** *Bulk sediment ages from core MD04-2832. Errors reported as 1σ.*

						At point of deposition	
Laboratory Code	**Depth (cm)**	**F_{modern}**	**$\Delta^{14}C$ (‰)**	**^{14}C Age (yr BP)**	**Deposition Age (Cal BP)**	**F_{modern}**	**^{14}C Age (yr BP)**
SUERC-93728	1.5	0.90 ± 0.004	-102.26 ± 1.72	821 ± 35	-56	0.90	877
SUERC-93729	11.5	0.84 ± 0.004	-164.04 ± 1.72	1396 ± 35	-36	0.84	1432
SUERC-93730	36.5	0.81 ± 0.004	-192.94 ± 2.12	1676 ± 35	21	0.81	1655
SUERC-93735	65.5	0.82 ± 0.004	-184.84 ± 0.62	1608 ± 35	94	0.83	1515
SUERC-93736	80.5	0.81 ± 0.004	-197.02 ± 0.51	1730 ± 35	149	0.82	1582
SUERC-93737	105	0.82 ± 0.004	-185.03 ± 1.22	1605 ± 35	244	0.84	1361
SUERC-93738	125.5	0.81 ± 0.004	-192.05 ± 2.12	1668 ± 35	318	0.85	1350
SUERC-93739	135.5	0.81 ± 0.004	-194.08 ± 3.13	1677 ± 38	355	0.85	1323
SUERC-93740	185.5	0.78 ± 0.004	-220.02 ± 1.42	1956 ± 37	536	0.84	1420
SUERC-93744	265.5	0.74 ± 0.004	-262.30 ± 2.82	2394 ± 37	850	0.83	1546

321

322 The comparison of the OC content and modern OC show minimal OC_{petro} inputs (< 0.1 %) to
323 the fjord sediments (Suppl.Fig.4). The catchment of Loch Sunart is dominated by metamorphic
324 and igneous geology; therefore, low OC_{petro} input is expected. The relatively minimal amounts
325 of OC_{petro}, in comparison to the total OC content, suggests that biospheric (terrestrial and
326 marine) OC from the late Holocene (Table 2) is the primary factor determining the composition
327 and age of the OC in these sediments.

328

329 **4.3 Bulk and Organic Geochemistry**

330 The OC content of the sediment varies between 2 to 3% down-core, with much of the variation
331 largely driven by the origin of OC (Fig. 3A). Up to 1584 ± 58 AD there was little variation in
332 C/N ratios or $\delta^{13}C_{org}$ values, with mean values of 11.42 ± 0.57 and -20.16 ± 0.9 ‰ respectively.
333 Using these values, in conjunction with the BIT index (Fig. 4G), it was estimated that 8.47 ±
334 1.56 % of the total OC originates from terrestrial sources (Fig. 3G). At 1584 ± 58 AD the C/N
335 ratio increased, peaking at 16.8 in 1802 ± 45 AD, while the $\delta^{13}C_{org}$ values were increasingly
336 depleted with values as low as -24.98 % at 1802 ± 45 AD (Fig. 3C). These changes reflect of
337 increased inputs of OC_{terr}; estimates from the mixing model indicated that the highest inputs
338 represented 28.29 ± 3.03 % of the total OC in sediments being derived from the terrestrial
339 environment. Both the C/N ratios and $\delta^{13}C_{org}$ values begin to return to the pre-1584 AD levels

after the main peak yet OC_{terr} input remains higher today (~10%) than that observed at the start of the record.

The TGA data (Fig. 3E) shows that the increased OC entering the system is associated with OM_L and OM_{recal}. The OM_L shows a slight increase across the period of increased OC_{terr} input likely due to surficial soils and vegetation flowing into the fjord. The OM_{recal} shows the greatest increase, which indicates that the OC_{terr} entering the sediments, is sourced from a degraded pool of OM in the catchment likely deep soils. This is supported by the $\Delta^{14}C$ data that shows that the OC entering the system during this period of increased OC_{terr} is aged suggesting the erosion of older (possibly deeper) soils (Fig. 3D).

Metal concentrations vary little in the first 500 years of the record; there are two small peaks observed within Lead (Pb), Copper (Cu) and Zinc (Zn) data at ~1500 and 1650 AD potentially related to the initial phase of soil erosion and or small scale (individuals) mining for smelters within the catchment (Fig. 3). The quantity of Pb entering the sediment dramatically increases at 1766 ± 25 AD which corresponds to the initiation of Pb mining in the catchment (Fig. 2). The increase in Pb found in the sediment is sustained past the closure of the mines indicating that the mining practices activated a source of Pb that is persistent and is still supplying material to the sediments. The presence of high Pb concentration beyond the peak time of mining impact could potentially be linked to the introduction of leaded fuel in the early 20^{th} century, which has been shown to pollute sedimentary systems in Scotland (Rose et al., 2012). The concentrations of Cu and Zn peak later in the record (~1900 AD) as those metals begin to be actively mined (Fig. 2).

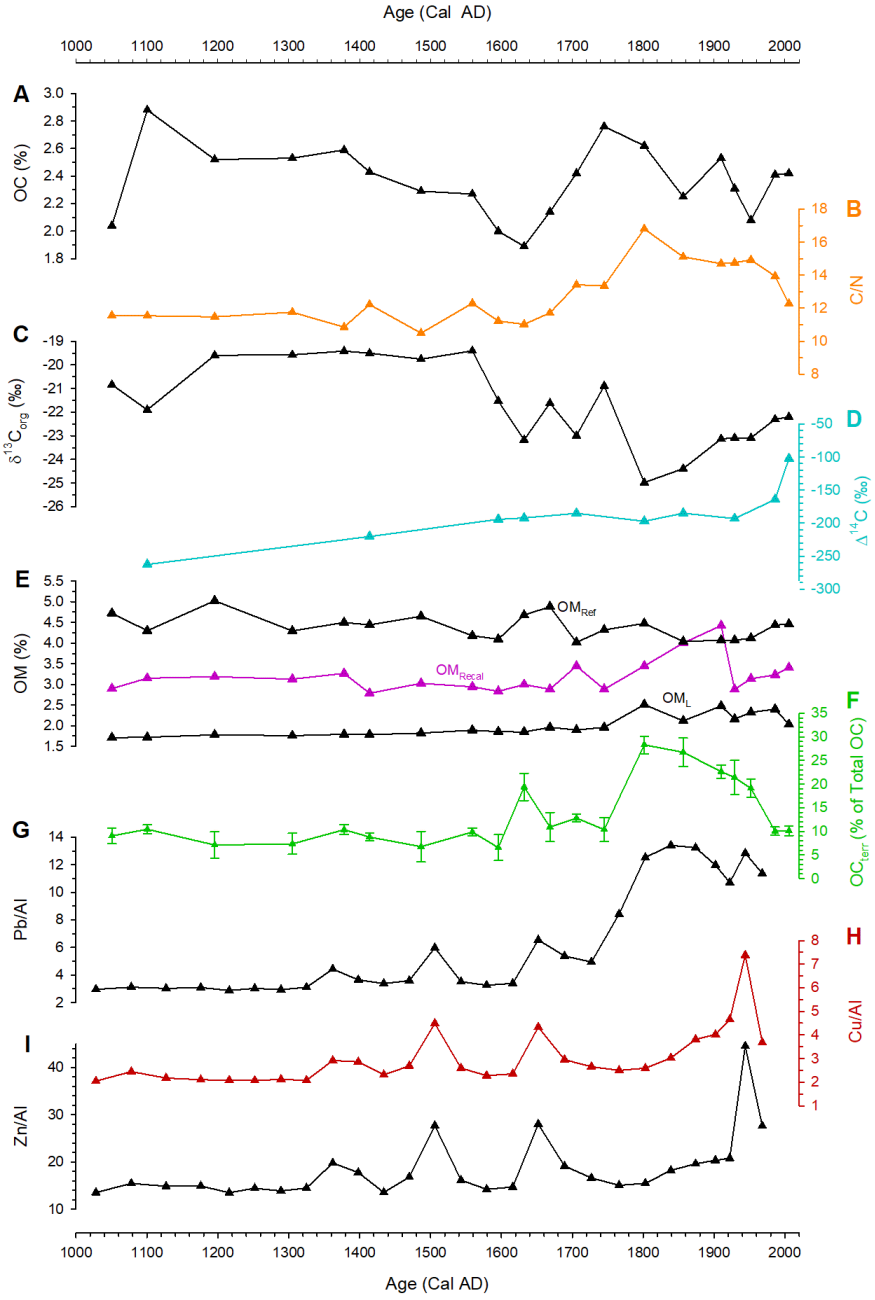

361

362 **Figure 3.** Downcore bulk and inorganic geochemical profiles for core MD04-2832. (**A**) OC
363 content (%). (**B**) C/N ratio. (**C**) $\delta^{13}C_{org}$ (‰). (**D**) $\Delta^{14}C$ (‰) of the OC. (**E**) OM content (%) of
364 the sediments broken into three thermal fractions describing biodegradability: labile (OM_L),
365 recalcitrant (OM_{recal}) and refractory (OM_{Ref}). (**F**) OC_{terr} (% of total OC) calculated from the
366 Bayesian mixing model (*Section 3.4*) (**G**) lead/aluminium ratio. (**H**) copper/aluminium ratio.
367 (**I**) zinc/aluminium ratio.

368

369

The organic geochemical measurements (Fig. 4) support the bulk measurements with them all showing increased input of OC_{terr} to the fjord sediments in the latter half of the record. The ALK C_{25-35} and LCFA are associated with higher terrestrial vascular plants, the values observed at the start of the record show little variation prior to 1584 ± 58 AD with mean values for this period of 113.6µg gOC^{-1} and 0.33 mg gOC^{-1} respectively, suggesting a low but steady input of OC_{terr} (Fig. 3G). As with bulk measurements, both the ALK C_{25-35} and LCFA show significant increases peaking at 339.3 µg gOC^{-1} and 1.20 mg gOC^{-1} in 1802 ± 45 AD which is indicative of significantly greater quantities of terrestrial vegetation entering the fjord. The majority of this terrestrial vegetation derived OC is likely entering the fjord from soils with a far smaller fraction originating from fresh (labile) vegetation as the increase in OM input during this period is driven by the OM_{recal} fraction opposed to the OM_L (Fig. 3E).

This upward trend in the latter half of the record are mirrored in the TAR_{FA} , which indicate an increase of OC_{terr} input. TAR_{FA} values of 1 suggest equal quantity of terrestrial and aquatic input (Bianchi and Canuel, 2011; Meyers, 1997), the TAR_{FA} values observed are < 1 which specifies that the OC is originates from marine sources (Fig. 4F). The increase in TAR_{FA} after 1584 ± 58 AD indicates that OC_{terr} input increases but OC_{mar} remains the dominant source of OC at the site which supports the outputs from the Bayesian mixing model (Fig. 3F).

The BIT index strongly correlates (R^2 = 0.95) with branched GDGTs (I+II+III) which are terrestrially derived (Smith et al., 2010) (Fig. 5A). Further, there is no correlation between the BIT Index and crenarchaeol concentrations suggesting OC_{mar} input through the last 1000 years has been consistent, which indicates that the variation in the BIT index observed is due to increases in OC_{terr} input (Fig. 5B) further supporting the bulk and organic geochemical measurements.

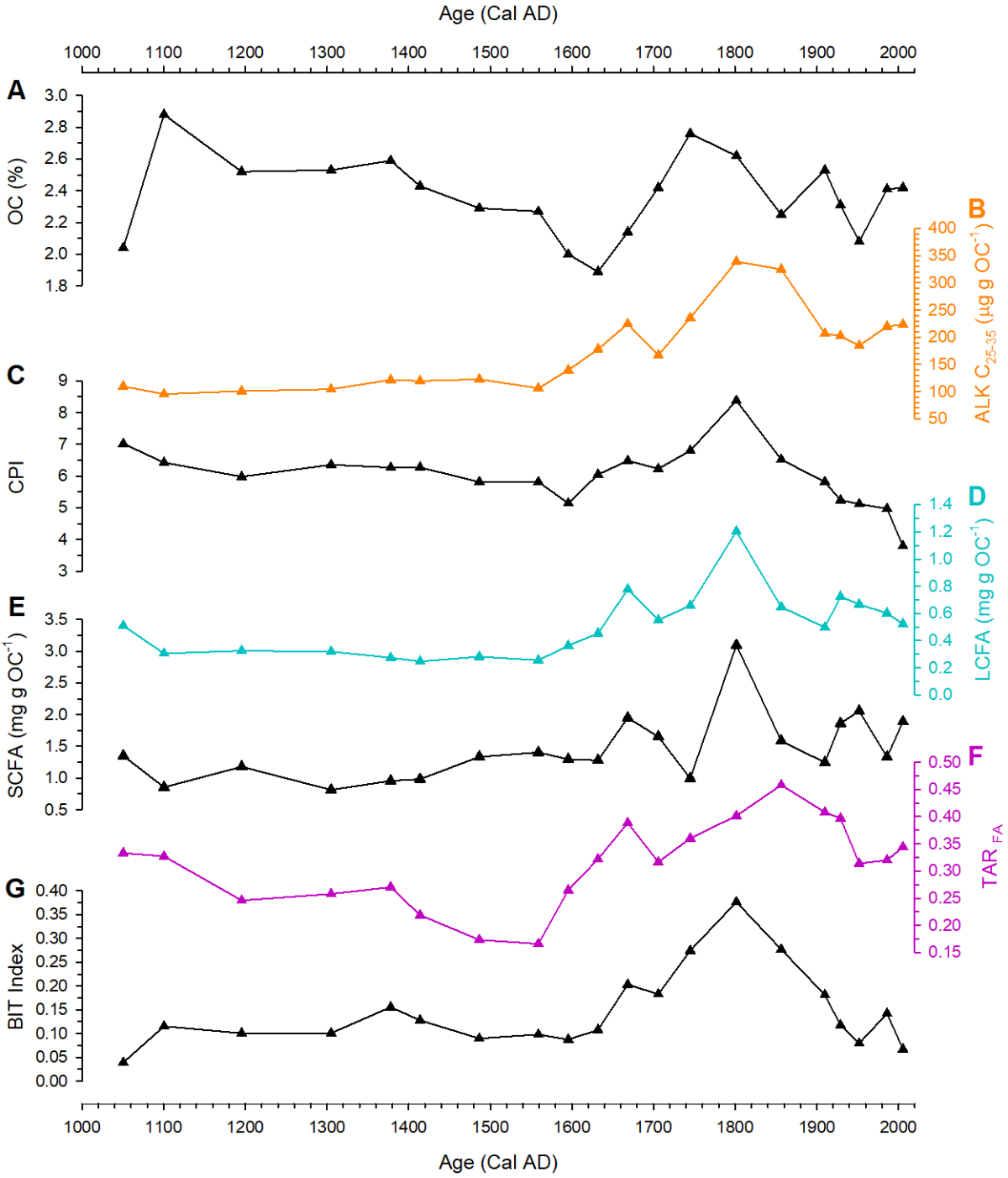

Figure 4. Organic geochemical profiles from core MD04-2832. (**A**) OC content (%). (**B**) Alkane $C_{25\text{-}35}$ (µg gOC^{-1}). (**C**) Carbon Preference Index (CPI). (**D**) long-chain fatty acids (mg gOC^{-1}). (**E**) short-chain fatty acids (mg gOC^{-1}). (**F**) fatty acid - terrestrial aquatic ratios. (**G**) branched isoprenoid tetraether index (BIT).

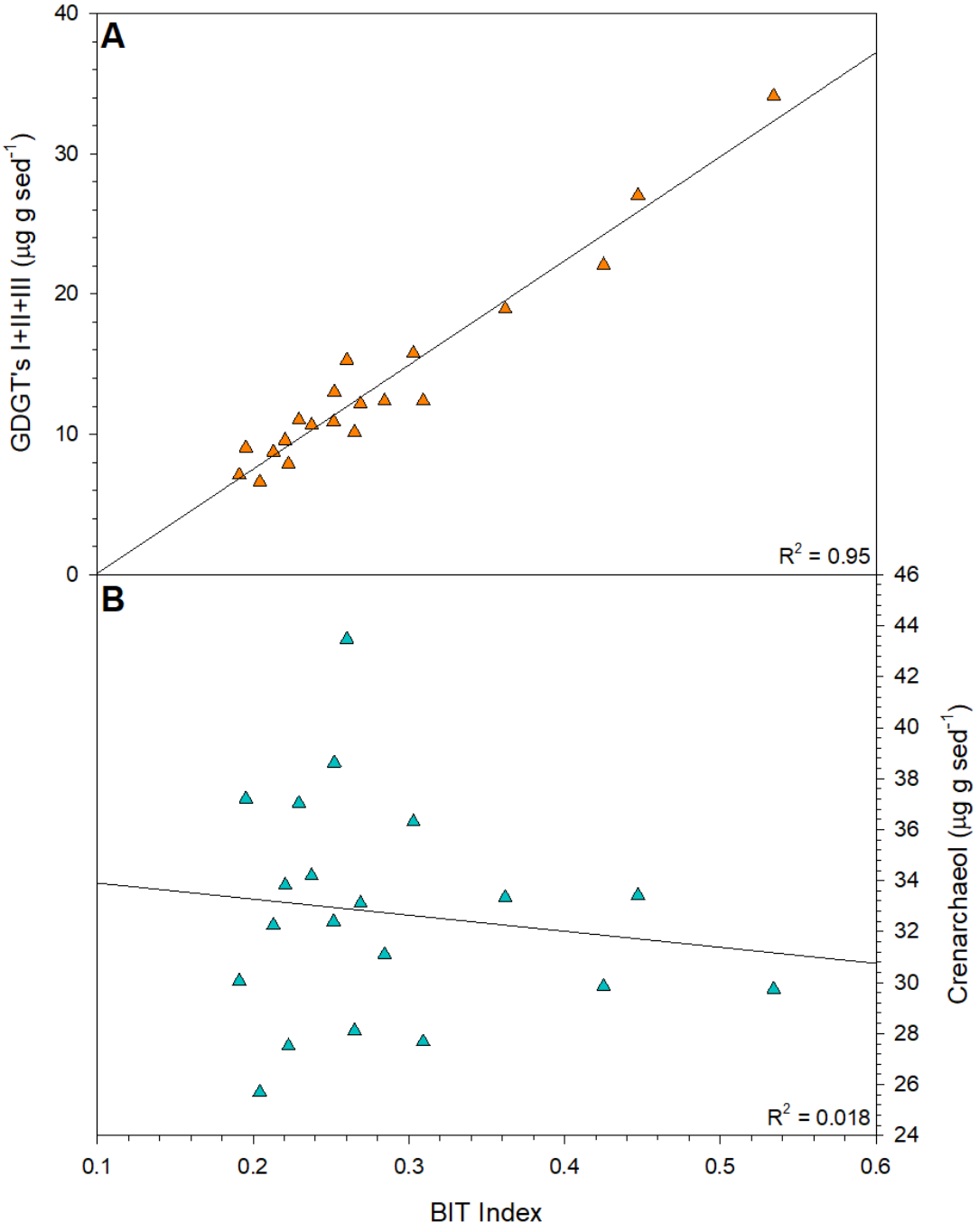

Figure 5. Binary plot illustrating the relationship between the BIT index and (**A**) Branched GDGTs (µg g sed^{-1}). (I + II +III) (**B**) Crenarchaeol concentration (µg g sed^{-1}).

The offset between the shell derived and the bulk OC ages provide an understanding of changes in input of aged OC at the time of deposition. If the OC being buried in sediments is fresh there should be minimal offset between the shell derived deposition age and bulk OC age, if older aged OC is entering the system the ages will diverge. The age offset between the shell and bulk

OC ages varies throughout the core (Fig. 6F) suggesting that aged OC input to the sediment (likely from soils) is present throughout the last 1000 years. Yet the quantity of aged OC entering the system has changed. The offset between the shell and OC ages begins to increase at 135 cm (~1597 AD) corresponding to the increased OC_{terr} input (Fig. 6B) potentially driven by deep soil erosion containing aged OC (Fig. 6). During this period of increased OC_{terr} input the age offset increases, peaking at 1634 years at 36.5 cm (~1930 AD) suggesting the continual input of old (potentially deep) soil deposits. As the OC_{terr} input decreases towards the core top, the age offset reduces to 932 years potentially indicating reduction in soil erosion and recovery of the catchment to pre-disturbance values (Fig. 6F).

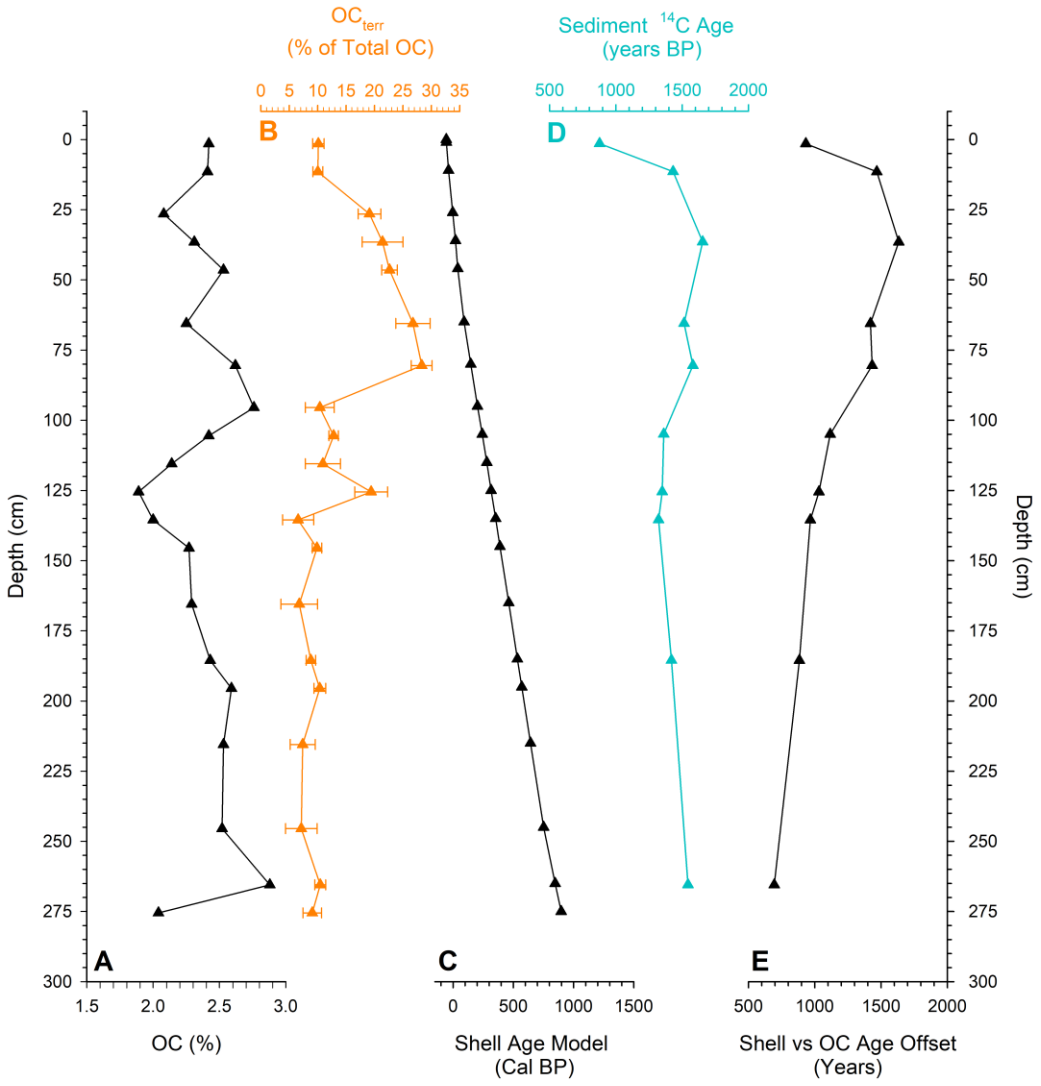

Figure 6. Comparison of the age of the OM versus the time of deposition (Shell derived age model). (**A**) OC content (%). (**B**) OC_{terr} (% of total OC) calculated from the Bayesian mixing model (*Section 3.4*) **(C)** Output from Bayesian age model (Cal BP) **(D)** Conventional ^{14}C age of the OC at the point of deposition (years BP) (**E**) Age offset between the age model (Shell) and the OC (years).

4.4 Sedimentation and Carbon Accumulation

The mean sedimentation rate at site MD04-2832 is 0.27 ± 0.05 cm yr^{-1} (Fig. 7B) which is broadly comparable to the Holocene norm of Loch Sunart (Smeaton et al., 2016) and similar to that observed in other vegetated fjords globally (Bianchi et al., 2020; Syvitski and Shaw, 1995). The record is punctuated by several shifts in this rate; the period between 1000 – 1200 AD is characterised by a lower very stable sedimentation rate of 0.20 ± 0.01 cm yr^{-1}. There are three sharp increases in this rate occurring between 1565 – 1600 AD, 1700 – 1855 and 1915 – 1933 AD; with the sedimentation rates rising to 0.32 ± 0.01, 0.34 ± 0.02, 0.33 ± 0.02 cm yr^{-1} respectively. Interspersed between these increases the sedimentation rate decreases to the core average (0.27 ± 0.05 cm yr^{-1}).

The mean OCAR for the last 1000 years is 34.9 ± 10.2 gC m^{-2} yr^{-1} (Fig. 7C) which is at the upper end of OCARs recorded in vegetated fjords globally (Bianchi et al., 2020; Smith et al., 2015). The changes in sedimentation rate are mirrored in the OCAR with a peak of 65 gC m^{-2} yr^{-1} between 1700 – 1855. The peaks in OCAR correspond with rises in the terrestrial OCAR (Fig. 7C) suggesting that increased input of terrestrial material and OC are driving the variability in sedimentation rate and OCAR in the latter half of the record.

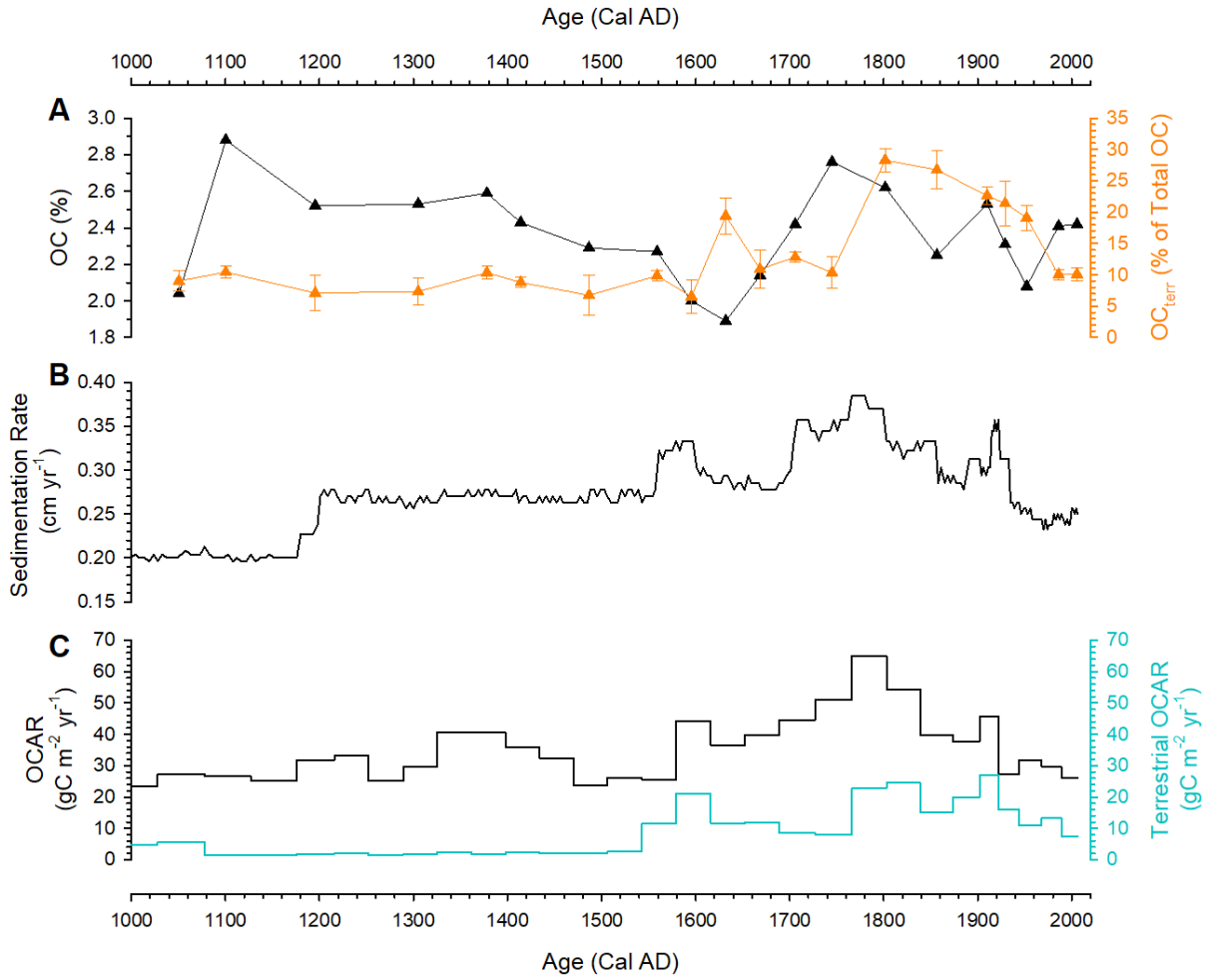

Figure 7. Sedimentation and OC accumulation over the last 1000 years. (**A**) Downcore profile of OC content (%) and OC_{terr} (% of Total OC) (**B**) Sedimentation rate (cm yr^{-1}) calculated using the Bayesian age model (Suppl. Fig. 3) and (**C**) OCAR and terrestrial OCAR (gC m^{-2} yr^{-1}).

5. The Evolution of a Sedimentary C Store

The latter half (1580 AD onwards) of the last millennium witnessed a 20 % rise in OCAR, above that observed in the preceding 500 years with 80 % of that extra OC originating from the terrestrial environment. The observed increases in OC_{terr} (Fig.3) do not directly correspond to any major change in climate (Cage and Austin, 2010; Rydval et al., 2017) and relative sea level (RSL) change had slowed significantly by this time (Shennan et al., 2018). Therefore, the increase in terrestrial OC seems to be de-coupled from either driver (i.e. climate, RSL), suggesting another mechanism had become dominant during this period of time. The last millennium witnessed an unprecedented anthropogenic pressure on the catchment (Fig. 2) to

provide resources for a growing local and national population in Scotland (Suppl. Fig. 9). Our sediment records show that anthropogenic disturbances to the catchment were initiated at approximately 1580 ± 63 AD, when there is a significant increase in terrestrial input (Fig. 3). The proportion of OC_{terr} to total OC content rose from less than 7% at the start of the record to a maximum of 28 % by 1802 AD. During the 16th Century scrub vegetation was being removed from the landscape to improve grazing and to supply local charcoal production (Tipping, 2013), which in turn reactivated lower slope erosion (Brazier and Ballantyne, 1989), mobilizing and transporting aged OC_{terr} to the fjord sediments (Fig. 6).

In Loch Sunart, the initial phase of the 16th Century disturbance resulted in a pulse of coarse grained mineralogical material being delivered to the sediments, most likely due to the erosion of deep soils (Ballantyne, 1991; Brazier and Ballantyne, 1989) as observed in an increase in grain size and magnetic susceptibility at this time (Suppl. Fig. 5). This high mineralogical input resulted in a dilution effect, lowering the OC in the fjord sediment. The initial pulse was followed by an increased input of terrestrial OC (1584 ± 58 AD), as evidenced by a decrease in $\delta^{13}C_{org}$ from -18.5 ‰ to -25.0 ‰ and an increase in C/N, BIT index (Figs. 3 & 4). During this period the age of the OC significantly diverges from the age of deposition (shell-derived age model) indicating the OC_{terr} entering the system is aged which suggests erosion of older, deeper soil within the catchment (Fig. 6), possibly linked to slope destabilization due to scrub removal (Ballantyne, 1991; Brazier and Ballantyne, 1989). This pattern is comparable to a similar record in Loch Etive (Nørgaard-Pedersen et al., 2006), which showed a marked increase in OC coupled to an increase in magnetic susceptibility over the last 1,000 years, which is indicative of higher mineralogical input suggesting a terrestrial source. This shift towards greater terrestrial input is further supported by the biomarker profiles, which all indicate an increase in terrestrial OC input to the sediments (Fig. 4), these complementary records presumably reflect regional terrestrial responses across NW Scotland.

A decline in OC_{terr} inputs to the sediments of Loch Sunart in the early to mid-1800s suggests the fjord system is potentially returning to pre-1580 conditions based on chemical biomarkers and bulk OC proxies (Figs. 3 & 4). Further, the age offset between the shell derived age model and the age of the OM within the upper most sediments has reduced to pre-disturbance values suggesting a reduction in aged OC input (Fig. 6). These changes could be due to the exhaustion of erodible soil materials (aged OC), or more likely that the depopulation of the catchment during the 19th century (Suppl Fig. 9) allowed the recovery of vegetation and stabilization of the soils within the catchment. More recent disturbance of the catchment has also impacted the

quantity of OC held within fjord sediments. In particular, the widespread planting of coniferous woodland for timber production starting in 1927 and accelerating during the 1950s is likely associated with increased OC_{terr} inputs from this time onward (Fig. 7). Prior to the 1970s before tree planting occurred all sites were cultivated which typically involved ploughing and furrows being cut (Carling et al., 2001) resulting in hydrologically sensitive soils where OC_{terr} could be easily mobilized (Moffat, 1988). A pulse of slightly coarser-grained (Suppl. Fig.5) material diluted the bulk OC concentration in the sediments and was followed rapidly (1964 ± 8 AD) by a marked increase in OC_{terr}. Interestingly, this initial response of OC dilution, via coarse lithic material input from eroding soils, is similar to that observed during the 1580 AD event.

The pressure humans have exerted, and the associated disturbance of vegetation and soils within the catchment from the late 18th Century to the present day through Pb, Zn and Cu mining alongside commercial forestry, is several orders of magnitude more intense than prior to the 1580 AD. For example, the concentrations of these metals found in the sediment increases dramatically (Fig. 3) from around the mid-1700s, intensifying in the 1900s and corresponds to the written records for mining activity in and around Stontian, within the Loch Sunart catchment (Smout, 1993; Tipping, 2013). Yet the terrestrial response to these later catchment alterations are muted in comparison (Fig. 7). It is therefore unlikely that human activity was the sole driver of this increased terrestrial C storage within the sediments during the 16th Century. Here, we hypothesis that abrupt climatic change may have been the contributing factor responsible for the initiation of heightened terrestrial responses to disturbance as observed in other Scottish coastal systems (Mao et al., 2020). For example, at approximately 1525 AD there was a rapid reorganization in the NAO recorded in the sediments of Trondheimsfjord, Norway (Faust et al., 2016), where the NAO switched to a positive phase after a sustained period (~315 years) in its negative phase. This positive switch was short (10-15 years) but would have created a wetter atmosphere over NW Europe. Moreover, peatbog water table (Charman et al., 2006; Langdon et al., 2003) and tree ring temperature reconstructions (Rydval et al., 2017) from Scotland confirm this widespread atmospheric reorganization and corroborate a transition to a wetter environment. Loch Sunart has been shown to be sensitive to NAO-forcing (Gillibrand et al., 2005), whereby the switch in the phase of NAO recorded in the $\delta^{18}O$ record (Cage and Austin, 2010) may also have driven increased runoff, and increased OC_{terr} loss through soil erosion. This link between regional climates, oceanography and $\delta^{18}O$ was outlined in Scottish fjords by (Cage and Austin, 2010) in their interpretation of a millennial-scale record from Loch Sunart. In particular, during the dry

519 negative NAO phases of the Holocene, the catchment would build and store soil materials,
520 which could then quickly be lost during the shift to a positive, wetter phase of the NAO (Trouet
521 et al., 2009). The major reorganization in the mode of the NAO over the North Atlantic during
522 the late Holocene may have triggered this enhanced terrestrial response. We hypothesize that
523 the long-term modification of the terrestrial environment by humans sensitized the catchment
524 to abrupt climatic reorganization. The shift in the NAO with the associated anthropogenic
525 destabilization resulted in a more vulnerable terrestrial ecosystem, allowing for the
526 mobilization and transfer of both contemporary and aged OC_{terr} to the fjord sediments (Fig. 6).

527 The last millennium has seen two significant increases in sedimentation rate (Fig. 7) associated
528 with the increasing anthropogenic pressure, potentially twinned with earlier climate instability
529 in the mid-16th century (Cage and Austin, 2010; Faust et al., 2016) and during the
530 industrialization of the catchment (~1750 AD). Both increases in sedimentation rates are
531 mirrored by an increase in OCAR; these increases are driven by OC_{terr} input, which can be
532 large and rapid. Yet given time the OCAR return to pre-disturbances norms suggests the
533 catchment is recovering and retaining a greater quantity of OC_{terr}. This demonstrates that fjord
534 sediments not only record changes in climate and the catchment, but if OC supply increases
535 these systems are responsive and have the capacity to capture and bury OC at greater rate than
536 the long-term Holocene norm (Smeaton et al., 2016).

537 **6. Conclusion**

538 While fjords are known hotspots for C burial (Smith et al., 2015) and storage (Smeaton et al.,
539 2017), the effectiveness of these environments as highly responsive long-term OC sinks is now
540 evident from this study. It is clear that anthropogenic pressure is a key driver in the
541 development of such coastal C stores over the last millennium. The results indicate that
542 increasing human activity within the catchment drove changes in the terrestrial environment
543 and the knock-on transport of OC_{terr} to the coastal ocean. The unique geomorphology and
544 oceanographic conditions (Bianchi et al., 2020; Howe et al., 2010) of the fjord allowed a large
545 proportion of the OC released by anthropogenic activity to be captured and stored before it
546 could be remineralised and lost to the marine environment and atmosphere. The observed
547 increase in burial rates during the period of terrestrial disturbance far exceed those seen earlier
548 in the record or through the Holocene (Smeaton et al., 2016) suggesting that fjords are highly
549 adaptable and capable of capturing greater quantities of OC and providing a greater climate
550 mitigation service if OC supply dictates. This adaptability of the coastal ocean, and fjords in

particular, in trapping terrestrial OC may represent an unrealized, yet significant long-term buffer in the global carbon cycle that will become increasingly important with the predicted increases in anthropogenic pressures and future climatic uncertainty.

Acknowledgments

This work was financially supported by the Natural Environment Research Council (grant number: NE/L501852/1), the EU FPV HOLSMEER project (EVK2-CT-2000-00060) and the EU FPVI Millennium project (contract number 017008), Biotechnology and Biological Sciences Research Council (grant number: BB/M026620/1) with additional support from the NERC Radiocarbon Facility (Allocation 1154.1005 and 2195.1019). We acknowledge Jon L. and Beverly A. Thompson Endowed Chair of Geological Sciences held by T.S. Bianchi in the Dept. of Geological Sciences at University of Florida, and China Scholarship Council for supporting part of this research. Further we thank both the SAGES (Scottish Alliance for Geoscience, Environment, Society) and MASTS (The Marine Alliance for Science and Technology for Scotland) pooling initiatives in funding this collaborative research. The CALYPSO long core was acquired by W. Austin within the frame of the French ECLIPSE programme with additional financial support from NERC, Scottish Association of Marine Science (SAMS) and the University of St Andrews. W. Austin and J. Howe would like to thank Marion Dufresne's Captain J.M. Lefevre, the Chief Operator Y. Balut (from IPEV). We would like to thank Charlie Wilson (SAMS) and Chris Wurster (University of St Andrews) for laboratory support. Lastly we would like to thank the editor and one anonymous reviewer for providing useful suggestions which have improved the manuscript.

Data Availability

Datasets related to this article can be found at https://doi.org/10.5285/60c437bd-9913-4c36-be71-b7b4b1751e26, hosted at National Geoscience Data Centre (NGDC) (Smeaton et al., 2021).

Author Contribution

C.S, X.C, T.S.B and W.E.N.A conceived the research and wrote the manuscript which all co-authors contributed data and provided input. The analytical work was undertaken by C.S, X.C

and A.G.C under the supervision of W.E.N.A, J.A.H and T.S.B. All authors contributed to manuscript revisions and final approval of the submitted version.

References

Appleby, P.G., 2002. Chronostratigraphic techniques in recent sediments, in: Tracking Environmental Change Using Lake Sediments. Springer, pp. 171–203.

Ascough, P., Cook, G., Dugmore, A., 2005. Methodological approaches to determining the marine radiocarbon reservoir effect. Prog. Phys. Geogr. 29, 532–547.

Ballantyne, C.K., 1991. Late Holocene erosion in upland Britain: climatic deterioration or human influence? The Holocene 1, 81–85.

Bao, R., McNichol, A.P., Hemingway, J.D., Gaylord, M.C.L., Eglinton, T.I., 2019. Influence of different acid treatments on the radiocarbon content spectrum of sedimentary organic matter determined by RPO/Accelerator Mass Spectrometry. Radiocarbon 61, 395–413.

Bianchi, T.S., Arndt, S., Austin, W.E.N., Benn, D.I., Bertrand, S., Cui, X., Faust, J.C., Koziorowska-makuch, K., Moy, C.M., Savage, C., Smeaton, C., Smith, R.W., Syvitski, J., 2020. Earth-Science Reviews Fjords as Aquatic Critical Zones (ACZs). Earth-Science Rev. 203, 103145. https://doi.org/10.1016/j.earscirev.2020.103145

Bianchi, T.S., Canuel, E.A., 2011. Chemical biomarkers in aquatic ecosystems. Princeton University Press.

Bianchi, T.S., Cui, X., Blair, N.E., Burdige, D.J., Eglinton, T.I., Galy, V., 2018. Centers of organic carbon burial and oxidation at the land-ocean interface. Org. Geochem. 115, 138–155.

Bishop, R.R., Church, M.J., Rowley-Conwy, P.A., 2015. Firewood, food and human niche construction: the potential role of Mesolithic hunter–gatherers in actively structuring Scotland's woodlands. Quat. Sci. Rev. 108, 51–75.

Blaauw, M., Christen, J.A., 2011. Flexible paleoclimate age-depth models using an autoregressive gamma process. Bayesian Anal. 6, 457–474.

Brazier, V., Ballantyne, C.K., 1989. Late Holocene debris cone evolution in Glen Feshie, western Cairngorm Mountains, Scotland. Earth Environ. Sci. Trans. R. Soc. Edinburgh 80, 17–24.

Brumsack, H.-J., 2006. The trace metal content of recent organic carbon-rich sediments: implications for Cretaceous black shale formation. Palaeogeogr. Palaeoclimatol. Palaeoecol. 232, 344–361.

611 Cage, A.G., Austin, W.E.N., 2010. Marine climate variability during the last millennium: The Loch
612 Sunart record, Scotland, UK. Quat. Sci. Rev. 29, 1633–1647.

613 Cage, A.G., Davies, S.M., Wastegård, S., Austin, W.E.N., 2011. Identification of the Icelandic
614 Landnám tephra (AD 871±2) in Scottish fjordic sediment. Quat. Int. 246, 168–176.

615 Cage, A.G., Heinemeier, J., Austin, W.E.N., 2006. Marine radiocarbon reservoir ages in Scottish
616 coastal and fjordic waters. Radiocarbon 48, 31–43.

617 Capel, E.., Arranz, J.M., Gonzalez-Vila, F.J., Conzalez-Perez, J.A., Manning, D.A.C., 2006.
618 Elucidation of different forms of organic carbon in marine sediments from the Atlantic coast of
619 Spain using thermal analysis coupled to isotope ratio and quadrupole mass spectrometry. Org.
620 Geo 37, 1983–1994. https://doi.org/10.1016/j.orggeochem.2006.07.025

621 Carling, P.A., Irvine, B.J., Hill, A., Wood, M., 2001. Reducing sediment inputs to Scottish streams: a
622 review of the efficacy of soil conservation practices in upland forestry. Sci. Total Environ. 265,
623 209–227.

624 Charman, D.J., Blundell, A., Chiverrell, R.C., Hendon, D., Langdon, P.G., 2006. Compilation of non-
625 annually resolved Holocene proxy climate records: stacked Holocene peatland palaeo-water
626 table reconstructions from northern Britain. Quat. Sci. Rev. 25, 336–350.

627 Cui, X., Bianchi, T.S., Hutchings, J.A., Savage, C., Curtis, J.H., 2016a. Partitioning of organic carbon
628 among density fractions in surface sediments of Fiordland, New Zealand 1016–1031.
629 https://doi.org/10.1002/2015JG003225.Received

630 Cui, X., Bianchi, T.S., Savage, C., 2017. Erosion of modern terrestrial organic matter as a major
631 component of sediments in fjords. Geophys. Res. Lett. 44, 1457–1465.

632 Cui, X., Bianchi, T.S., Savage, C., Smith, R.W., 2016b. Organic carbon burial in fjords : Terrestrial
633 versus marine inputs. Earth Planet. Sci. Lett. 451, 41–50.
634 https://doi.org/10.1016/j.epsl.2016.07.003

635 Dadey, K.A., Janecek, T., Klaus, A., 1992. Dry bulk density: its use and determination. Proc. Ocean
636 Drill. Program, Sci. Results 126, 551–554.

637 Danielson, R.E., Sutherland, P.L., 1986. Porosity, in: Methods of Soil Analysis, Part 1, Physical and
638 Mineralogical Methods. pp. 443–461.

639 Faust, J.C., Fabian, K., Milzer, G., Giraudeau, J., Knies, J., 2016. Norwegian fjord sediments reveal
640 NAO related winter temperature and precipitation changes of the past 2800 years. Earth Planet.
641 Sci. Lett. 435, 84–93.

642 Fernandes, R., Millard, A.R., Brabec, M., Marie-Josee, N., Grootes, P., 2014. Food Reconstruction

643 Using Isotopic Transferred Signals (FRUITS): A Bayesian Model for Diet Reconstruction.
644 PLoS One 9, 1–9. https://doi.org/10.1371/journal.pone.0087436

645 Folk, R.L., 1954. The distinction between grain size and mineral composition in sedimentary-rock
646 nomenclature. J. Geol. 62, 344–359.

647 Galy, V., Beyssac, O., France-Lanord, C., Eglinton, T., 2008. Recycling of graphite during Himalayan
648 erosion: a geological stabilization of carbon in the crust. Science (80-.). 322, 943–945.

649 Gillibrand, P.A., Cage, A.G., Austin, W.E.N., 2005. A preliminary investigation of basin water
650 response to climate forcing in a Scottish fjord : evaluating the influence of the NAO. Cont. Shelf
651 Res. 25, 571–587. https://doi.org/10.1016/j.csr.2004.10.011

652 Harris, D., Horwa, W.R., Kessel, C. Van, 2001. Acid Fumigation of Soils to Remove Carbonates
653 Prior to Total Organic Carbon or Carbon-13 Isotopic Analysis. Soil Sci. Soc. Am. J. 65, 1853–
654 1856. https://doi.org/10.2136/sssaj2001.1853

655 Heaton, Timothy J, Köhler, P., Butzin, M., Bard, E., Reimer, R.W., Austin, W.E.N., Ramsey, C.B.,
656 Grootes, P.M., Hughen, K.A., Kromer, B., Reimer, P.J., Heaton, T J, 2020. Marine20 — The
657 marine radiocarbon age calibration curve (0-55,000 Cal BP). Radiocarbon 1–42.
658 https://doi.org/10.1017/RDC.2020.68

659 Hedges, J.I., Keil, R.G., 1995. Sedimentary organic matter preservation : an assessment and
660 speculative synthesis. Mar. Chem. 49, 81–115.

661 Heier-Nielsen, S., Conradsen, K., Heinemeier, J., Knudsen, K.L., Nielsen, H.L., Rud, N.,
662 Sveinbjörnsdóttir, Á.E., 1995. Radiocarbon dating of shells and foraminifera from the Skagen
663 core, Denmark: evidence of reworking. Radiocarbon 37, 119–130.

664 Howe, J.A., Austin, W.E.N., Forwick, M., Paetzel, M., Harland, R.E.X., Cage, A.G., 2010. Fjord
665 systems and archives : a review. Fjord Syst. Arch. Geol. Soc. London, Spec. Publ. 5–15.

666 Howe, J.A., Shimmield, T., Austin, W.E.N., Longva, O., 2002. Post-glacial depositional environments
667 in a mid-high latitude glacially-overdeepened sea loch , inner Loch Etive , western Scotland.
668 Mar. Geol. 185, 417–433.

669 Langdon, P.G., Barber, K.E., Hughes, P.D.M., 2003. A 7500-year peat-based palaeoclimatic
670 reconstruction and evidence for an 1100-year cyclicity in bog surface wetness from Temple Hill
671 Moss, Pentland Hills, southeast Scotland. Quat. Sci. Rev. 22, 259–274.

672 Lienkaemper, J.J., Ramsey, C.B., 2009. OxCal: Versatile tool for developing paleoearthquake
673 chronologies—A primer. Seismol. Res. Lett. 80, 431–434.

674 Liu, X., De Santiago Torio, A., Bosak, T., Summons, R.E., 2016. Novel archaeal tetraether lipids with

675 a cyclohexyl ring identified in Fayetteville Green Lake, NY, and other sulfidic lacustrine
676 settings. Rapid Commun. Mass Spectrom. 30, 1197–1205.

677 Mao, J., Burdett, H.L., McGill, R.A.R., Newton, J., Gulliver, P., Kamenos, N.A., 2020. Carbon burial
678 over the last four millennia is regulated by both climatic and land use change. Glob. Chang.
679 Biol. 26, 2496–2504.

680 Meyers, P.A., 1997. Organic geochemical proxies of paleoceanographic, paleolimnologic, and
681 paleoclimatic processes. Org. Geochem. 27, 213–250.

682 Moffat, A.J., 1988. Forestry and soil erosion in Britain–a review. Soil Use Manag. 4, 41–44.

683 Moossen, H., Abell, R., Quillmann, U., Bendle, J., 2013. Holocene changes in marine productivity
684 and terrestrial organic carbon inputs into an Icelandic fjord: Application of molecular and bulk
685 organic proxies. The Holocene 23, 1699–1710.

686 Nørgaard-pedersen, N., Austin, W.E.N., Howe, J.A., Shimmield, T., 2006. The Holocene record of
687 Loch Etive , western Scotland : Influence of catchment and relative sea level changes. Mar.
688 Geol. 228, 55–71. https://doi.org/10.1016/j.margeo.2006.01.001

689 Perdue, E.M., Koprivnjak, J.-F., 2007. Using the C/N ratio to estimate terrigenous inputs of organic
690 matter to aquatic environments. Estuar. Coast. Shelf Sci. 73, 65–72.

691 Ramsey, C.B., Lee, S., 2013. Recent and planned developments of the program OxCal. Radiocarbon
692 55, 720–730.

693 Rose, N.L., Yang, H., Turner, S.D., Simpson, G.L., 2012. An assessment of the mechanisms for the
694 transfer of lead and mercury from atmospherically contaminated organic soils to lake sediments
695 with particular reference to Scotland, UK. Geochim. Cosmochim. Acta 82, 113–135.

696 Rydval, M., Loader, N.J., Gunnarson, B.E., Druckenbrod, D.L., Linderholm, H.W., Moreton, S.G.,
697 Wood, C. V, Wilson, R., 2017. Reconstructing 800 years of summer temperatures in Scotland
698 from tree rings. Clim. Dyn. 49, 2951–2974.

699 Sepúlveda, J., Pantoja, S., Hughen, K.A., Bertrand, S., Figueroa, D., León, T., Drenzek, N.J., Lange,
700 C., 2009. Late Holocene sea-surface temperature and precipitation variability in northern
701 Patagonia, Chile (Jacaf Fjord, 44 S). Quat. Res. 72, 400–409.

702 Shennan, I., Bradley, S.L., Edwards, R., 2018. Relative sea-level changes and crustal movements in
703 Britain and Ireland since the Last Glacial Maximum. Quat. Sci. Rev. 188, 143–159.

704 Skei, J., 1983. Geochemical and sedimentological considerations of a permanently anoxic fjord—
705 Framvaren, south Norway. Sediment. Geol. 36, 131–145.

706 Smeaton, C., Austin, W.E.N., 2019. Where's the Carbon : Exploring the Spatial Heterogeneity of
707 Sedimentary Carbon in Mid-Latitude Fjords. Front. Earth Sci. 7, 1–16.
708 https://doi.org/10.3389/feart.2019.00269

709 Smeaton, C., Austin, W.E.N., 2017. Sources, Sinks, and Subsidies: Terrestrial Carbon Storage in Mid-
710 latitude Fjords. J. Geophys. Res. Biogeosciences 122, 2754–2768.
711 https://doi.org/10.1002/2017JG003952

712 Smeaton, C., Austin, W.E.N., Davies, A.L., Baltzer, A., Abell, R.E., Howe, J.A., 2016. Substantial
713 stores of sedimentary carbon held in mid-latitude fjords. Biogeosciences 5771–5787.
714 https://doi.org/10.5194/bg-13-5771-2016

715 Smeaton, C., Austin, W.E.N., Davies, A.L., Baltzer, A., Howe, J.A., Baxter, J.M., 2017. Scotland's
716 forgotten carbon : a national assessment of mid-latitude fjord sedimentary carbon stocks.
717 Biogeosciences 14, 5663–5674.

718 [dataset] Smeaton, C., Cui, X., Bianchi, T.S., Cage, A.G., Howe J.A., Austin, W.E.N. (2021):
719 Geochemical data for giant piston core MD04-2832 (Loch Sunart, Scotland). NERC EDS
720 National Geoscience Data Centre. https://doi.org/10.5285/60c437bd-9913-4c36-be71-
721 b7b4b1751e26

722 Smeaton, C., Hunt, C.A., Turrell, W.R., Austin, W.E.N., 2021. Marine Sedimentary Carbon Stocks of
723 the United Kingdom's Exclusive Economic Zone. Front. Earth Sci. 9.
724 https://doi.org/10.3389/feart.2021.593324

725 Smith, R.W., Bianchi, T.S., Allison, M., Savage, C., Galy, V., 2015. High rates of organic carbon
726 burial in fjord sediments globally. Nat. Geosci. 8, 450–453. https://doi.org/10.1038/NGEO2421

727 Smith, R.W., Bianchi, T.S., Savage, C., 2010. Comparison of lignin phenols and branched/isoprenoid
728 tetraethers (BIT index) as indices of terrestrial organic matter in Doubtful Sound, Fiordland,
729 New Zealand. Org. Geochem. 41, 281–290. https://doi.org/10.1016/j.orggeochem.2009.10.009

730 Smout, T.C., 2005. Oak as a commercial crop in the eighteenth and nineteenth centuries. Bot. J. Scotl.
731 57, 107–114.

732 Smout, T.C., 2004. History of the native woodlands of Scotland 1500-1920. Edinburgh University
733 Press.

734 Smout, T.C., 2003. People and woods in Scotland. Edinburgh University Press.

735 Syvitski, J.P.M., Burrell, D.C., Skei, J.M., 1987. Fjords: processes and products. Springer Science &
736 Business Media.

737 Syvitski, J.P.M., Shaw, J., 1995. Sedimentology and geomorphology of fjords, in: Developments in

738 Sedimentology. Elsevier, pp. 113–178.

739 Tipping, R., 2013. Towards an Environmental History of Argyll & Bute: A Review of Current Data,
740 Their Strengths and Weaknesses and Suggestions for Future Work.

741 Tipping, R., 1994. The form and the fate of Scotland's woodlands, in: Proceedings of the Society of
742 Antiquaries of Scotland. pp. 1–54.

743 Trouet, V., Esper, J., Graham, N.E., Baker, A., Scourse, J.D., Frank, D.C., 2009. Persistent positive
744 North Atlantic Oscillation mode dominated the medieval climate anomaly. Science (80-.). 324,
745 78–80.

746 USEPA, 2007. USEPA Method 6020A Inductively Coupled Plasma-Mass Spectrometry USEPA.
747 Washington DC.

748 USEPA, 1996. USEPA Method 3052 Microwave assisted acid digestion of sediments, sludges, soils
749 and oils Test Methods for Evaluating Solid Waste. Washington DC.

750 Van der Weijden, C.H., 2002. Pitfalls of normalization of marine geochemical data using a common
751 divisor. Mar. Geol. 184, 167–187.

752 Winchester, A.J.L., 1996. Scotland since Prehistory: Natural Change and Human Impact. Edited by
753 TC Smout. Pp. xx, 140. Aberdeen: Scottish Cultural Press.

754 Xu, X., Trumbore, S.E., Zheng, S., Southon, J.R., McDuffee, K.E., Luttgen, M., Liu, J.C., 2007.
755 Modifying a sealed tube zinc reduction method for preparation of AMS graphite targets:
756 reducing background and attaining high precision. Nucl. Instruments Methods Phys. Res. Sect.
757 B Beam Interact. with Mater. Atoms 259, 320–329.

758 Zillén, L., Conley, D.J., 2010. Hypoxia and cyanobacteria blooms-are they really natural features of
759 the late Holocene history of the Baltic Sea? Biogeosciences 7, 2567–2580.

760 Zillén, L., Conley, D.J., Andrén, T., Andrén, E., Björck, S., 2008. Past occurrences of hypoxia in the
761 Baltic Sea and the role of climate variability, environmental change and human impact. Earth-
762 Science Rev. 91, 77–92.

763